Materials Science Forum Vols. 215-216 (1996) pp. 13-20

On the Morphological Transition from Cellular to Planar Growth at High Solidification Velocity

A. Ludwig[1] and W. Kurz[2]

[1] Giesserei-Institut der RWTH, Intzestr. 5, D-52056 Aachen, Germany

[2] Laboratoire de Métallurgie Physique, EPFL, CH-1015 Lausanne, Switzerland

Keywords: Rapid Solidification, Absolute Stability, Morphological Transition, Plane Front, Elongated Cells

ABSTRACT

In the present paper the first experimental evidence for the absolute stability of a planar solid-liquid interface in a transparent organic alloy system is given. In-situ observations of the interface morphology of rapidly solidifying Succinonitrile-Argon alloys were performed. Reducing the solute content of the alloy, a morphological transition from deep cylindrical cells to a planar growth front was found. This transition developed in three different stages: (i) deep cells of circular cross section changed into a mixed pattern of elongated and cylindrical cells, (ii) which changed further into low amplitude cells and (iii) finally into the planar front. By increasing (decreasing) the solidification velocity, the elongated and cylindrical cells arranged themselves into larger structures which revealed the beginning of the transition to the planar front. For the low amplitude cells this transition could be observed directly by increasing (decreasing) the growth rate. These transitions are located in the region near the limit point of the neutral stability curve on the branch for absolute stability. Results of experiments and of linear stability theory agree within the limits of uncertainties in the materials properties and in the thermal gradient.

INTRODUCTION

The classical paper of Mullins and Sekerka in 1964 [1] predicted the growth of a morphologically stable planar solid-liquid interface above the so-called limit of absolute stability, V_{abs}. For small concentrations, the limit of constitutional undercooling, V_C, and the limit of absolute stability, V_{abs}, join in the V - C_0 plan to form a limit point located at (C_0*, V*). For alloys with a concentration smaller than C_0*, the interface should always be stable independent of the growth velocity.

In the last two decades the original analysis by Mullins and Sekerka has been extended in many ways. For example, Corriell and Sekerka [2] considered non-equilibrium effects at the liquid-solid interface. Their general expression for the velocity, concentration and temperature dependence of the distribution coefficient and the introduction of an expression considering attachment kinetics, led to the prediction that, at high velocities, where non-equilibrium conditions at the solid-liquid interface become important, the interface can not only be unstable with respect to steady morphological disturbances but also to oscillatory perturbations. Boettinger et al. [3,4] introduced a model for describing non-equilibrium effects on the liquidus slope. Using this model and the velocity dependence of the distribution coefficient [5], Davis et al. [6-8] studied the dependence of instabilities on solidification velocity for the thermal steady-state and the "frozen temperature approximation", i.e. equal thermal properties and vanishing latent heat. Recently, Huntley and Davis, have also included thermal effects [9].

A standard technique for the in-situ observation of the morphology of a solid-liquid interface is the solidification of transparent organic alloys. In the last two decades intensive studies of the dendritic and the cellular growth regimes in directional solidification as well as of the stability of the planar solid-liquid interface at low velocities were performed [10-12]. Trivedi et al. [13] investigated the solidification microstructure of a transparent organic alloy at high velocities in a thermal transient regime within a thin cell. They observed the transition from a dendritic to a fine cellular morphology with increasing velocity. A further increase of the growth rate could not be realised because of the tendency for thermal decomposition of the transparent material due to the necessary increase in the thermal gradient. Because of the experimental difficulties which occur at high growth rates, the direct observation of absolute stability has not yet been made.

In the present paper the morphological transitions around the limit point (C_0*, V*) are investigated by in-situ observations of the solidification patterns of bulk samples in the Succinonitrile (SCN)-Argon system. Long, fine tubes of square cross section, filled with different SCN-Ar alloys, were pulled rapidly from a furnace with essentially zero superheat into liquid coolant. Thus heat was extracted rapidly, resulting in solidification rates as high as 1.5 mm/s, which is one order of magnitude higher than that achieved until now. The solidification front inside the tube was observed in-situ through the coolant simultaneously from above and from the side with an optical microscope.

EXPERIMENTAL PROCEDURE

The capillary tubes used in this work had an internal cross section of 200 μm x 200 μm, 900 mm long, a wall thickness of 100 μm and were made of borosilicate glass. They were filled with SCN, which had to be distilled under vacuum and zone-refined with more than 50 passes to achieve the desired purity. The alloying was performed by applying different Argon-gas pressures to the molten SCN. The concentration of the alloy inside the tube was estimated by measuring the solid-liquid temperature interval ΔT_0 and referring to the SCN-Ar phase diagram from M.A. Chopra [14]. Details concerning the purification procedure, the estimation of the solute concentration and the solidification apparatus are given in [15].

Due to the small cross section of the capillary tube, the high withdrawal velocity and the efficient cooling, solidification within the tube took place nearly *perpendicular* to the side walls. The first solid was formed within the edges of the tube, as flat surface dendrites. After lateral impingement of the four surface dendrites from the edges, the solid-liquid interface revealed a pyramidal geometry with four planes. Whilst viewing from above, the microscope was focused on the bottom interface. Although the depth of focus was limited, cellular morphologies were also visible on the side planes. The distance between the side planes was approximately 100 μm, which was typical for the observation window used in the experiments (Fig.1).

Because of the flatness of the side planes of the pyramidal interface, the growth velocity could be regarded as constant and the solidification to be in steady state. The largest possible diffusion boundary layer in front of a solid-liquid interface is given by the boundary layer of a planar solidification front, $d_D = 2D/V$. For the solidification velocities realised in the experiments, d_D was

limited to $1.2 < d_D < 6$ µm with $D = 8.8 \times 10^{-10}$ m^2/s from [14]. Thus an overlap of the diffusion boundary layers from opposite side planes should only appear within the final solidification process, which is not relevant to the results presented in this publication.

Due to the four fold symmetry of the pyramidal interface and the fact that the crystal growth was perpendicular to the solid-liquid interface, the actual growth rate was obtained from the angle α between the interface normal and the axis of the tube, by: $V = V_0 \cos \alpha$, with V_0 the actual withdrawal velocity. Depending on the temperature of the cooling liquid, the resulting solidification velocity varied between $V = 0.3$ mm/s and 1.5 mm/s.

RESULTS AND DISCUSSION

By reducing the solute content of the alloy a morphological transition from deep cylindrical cells to a planar growth front was observed. Figure 1 shows exemples of the four different solidification morphologies which appeared by varying the Argon concentrations. For alloys with $\Delta T_0 = 415$ mK and above, an interface morphology consisting of cylindrical cells was found (a). At $\Delta T_0 = 280$ mK elongated cells appeared together with cylindrical ones (b). With $\Delta T_0 = 235$ mK the morphology

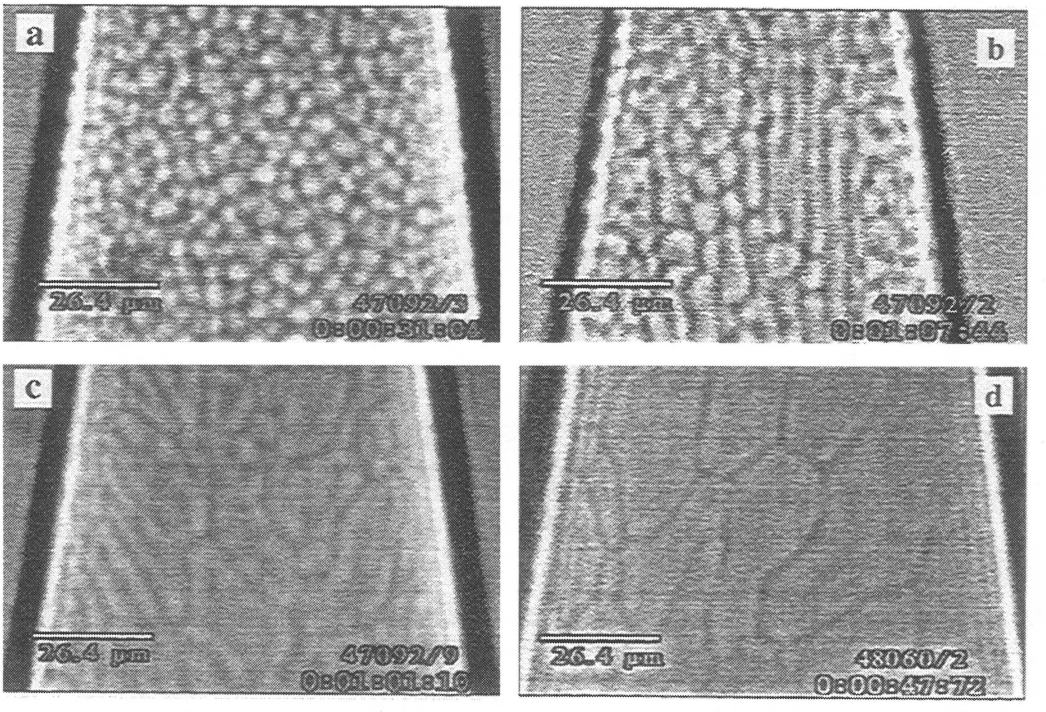

Fig. 1. Transition from a cellular interface morphology to a grain-like planar interface, achieved by reducing the concentration in the SCN-Ar alloy: (a) $\Delta T_0 = 415$ mK, (b) $\Delta T_0 = 280$ mK, (c) $\Delta T_0 = 235$ mK, (d) $\Delta T_0 = 60$ mK. The solidification velocities were similar, $V \approx 1.2$ mm/s.

changed to a coarse grain-like structure (c). The grain-like structure itself revealed a substructure indicated by the variation in the grey level. At $\Delta T_0 = 60$ mK the substructure disappeared and only the grain structure was observed (d). The solidification velocities were similar for all four cases ($V \approx 1.2$ mm/s). Assuming Ar as the only solute and considering a constant distribution coefficient k and constant liquidus slope m, with $k = 0.2$ and $m = -4.7$ K/wt.% [14], the alloy with $\Delta T_0 = 415$ mK contained $C_0 = 221$ wt.ppm Argon.

The size of the structures, where cylindrical cells together with elongated cells were present (fig. 1b), decreased with increasing velocity. For the same solidification velocity, the width of the elongated cells was comparable to the diameter of the cylindrical cells. The relative amount of elongated cells increased with increasing solidification rate. At low and at high solidification velocities, relatively large areas with irregular appearance were observed. These areas, as well as some elongated and cylindrical cells at small velocities, revealed a substructure. The orientation of the elongated cells changed slightly during an experimental run. Usually the elongated cells were aligned within an angle of 15° around the withdrawal direction, but sometimes the orientation of the elongated cells differed markedly from the withdrawal direction.

The substructure in figure 1c) shows curved and ring-shaped configurations. Sometimes only a dark shadowing in the centre of the grain-like structure was found. At low and high solidification velocities the substructure disappeared. The size of the substructure was estimated to $\lambda = 4.7$ µm. Surface dendrites were found to be at the origin of the grain-like structure (fig. 1c-d). Further details about the formation of the grain-like structure are given in [15] and on the surface dendrites in [16].

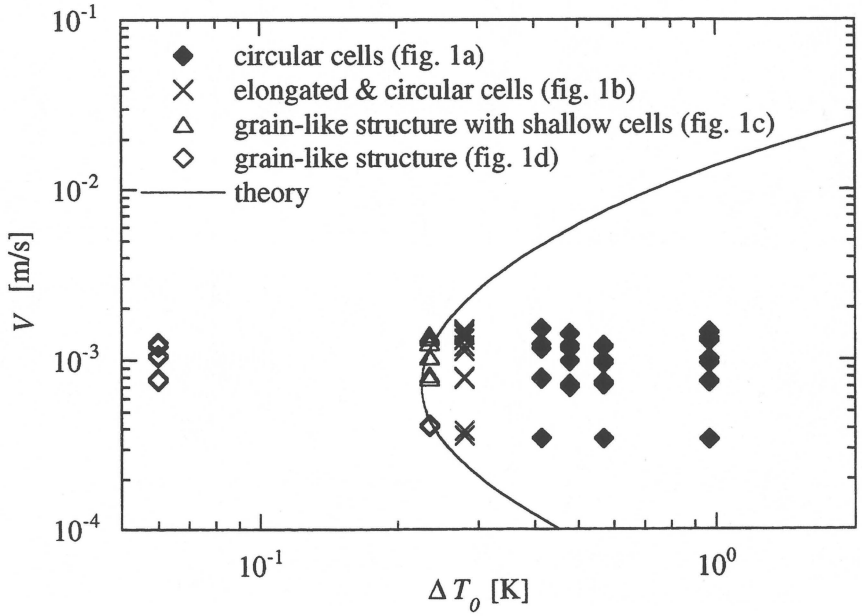

Fig. 2. For $G_L = 5 \times 10^4$ K/m and $D = 6 \times 10^{-10}$ m^2/s the neutral stability curve correlated best with the experimental observations. Note that the measuring error was ± 40 mK for small ΔT_0 and ± 70 mK for the larger ones. The measuring error for V was less than ± 0.07 mm/s.

Figure 2 summarises the experimental results in a V-ΔT_0 diagram by using four different types of markers to indicate the morphological changes. To compare the experimental results with the theoretical predictions, the neutral stability curve was calculated using the model of Huntley and Davis [9]. This model considers non-equilibrium effects at the interface due to Boettinger et al. [3,4] and Aziz [5], although, for the growth rates which occurred in our experiments, local equilibrium should be a reliable assumption. Thus oscillatory instabilities are neither expected nor observed. The material properties utilised in the calculations are given elsewhere [15]. The most critical parameters for the comparison between experiments and theory are the diffusion coefficient D and the interfacial temperature gradient in the liquid, G_L. Chopra calculated D from different theoretical diffusion models [14]. Thus D was assumed to be limited to 5.3×10^{-10} m^2/s $< D < 11 \times 10^{-10}$ m^2/s. G_L could be approximated by assuming a linear temperature distribution between the centre axis of the tube (which is assumed to be still at the temperature of the heater, T_h) and the solid/liquid interface. For alloys with $\Delta T_0 = 235$ mK, G_L was 10^4 K/m. This value must be regarded as a rough approximation because with an error function profile instead of a linear relation, G_L can be quite larger and with a lower temperature at the centre axis than T_h, G_L can largely be eliminated.

Assuming that (1) the grain structure without the substructure represents the plane front and (2) the substructure in the grain-like structure represents shallow perturbations growing just above the limit of stability, the neutral stability curve for $G_L = 5 \times 10^4$ K/m and $D = 6 \times 10^{-10}$ m^2/s correlated well with the experimental observations. The first assumption can be justified by the fact, that the grains are created from surface dendrites growing at the tube walls, even for the material with the highest purity ($\Delta T_0 = 60$ mK). This might be due to recrystallisation. The second assumption is confirmed by the fact, that the critical wave length calculated for the onset of instability is similar to the size of the substructure. Although the measuring error of this quantity was large the agreement is quite good. The above values for G_L and D, which gave the best fit to the experimental points, are in the expected range.

Elongated cells were first observed in 1955 by Walton et al. [17]. They performed decantation experiments with dilute alloys (Sn-Pb) at the limit of constitutional undercooling. In this study and, in more detail, in their following investigation of the solidification of dilute Pb-Sn, Pb-Ag, Pb-Au alloys [18], they stated that in the transition region, the interface developed a pox-like structure as a stage of development prior to cell formation. The cells first appeared to be irregular and elongated. Further approaching the cellular region, the elongated cells subdivided to form smaller, almost regular, cells. In addition they found, that the direction of the elongated cell boundary coincided with a (111) trace on the interface - the orientation of the elongated cells revealed the underlying crystal orientation. At a grain boundary the elongated cells formed a well defined angle (see fig. 13 of ref. [18]). A solidification pattern similar to their figures 12, 15-16 are also found in our experiments.

Biloni reported the appearance of pox-like structures and elongated cells in dilute aluminium (Al-X) [19] and tin (Sn-Pb,Sn-Sb) alloys [20,21]. Similar observation for dilute solutions of ammonium fluoride in water were made by Jones [22]. Cole and Winegard showed that elongated cells can also appear in dilute ternary alloys (Sn-Pb-Sb) [23]. The effect of crystal orientation on the initial non-planar interface morphology were investigated by Morris and Winegard in more detail for a dilute Pb-Sb alloy [24]. They found, that when the growth direction was near a [100] or [111] nodes developed. Near [110] elongated cells developed. Experimental observations of pox and elongated

cells in dilute Al alloys (Al-Cu, Al-Ti, Al-Cr, Al-Zn) were described in a series of publications by Sato and Ohira [25-28]. Tewari and Chopra observed elongated perturbations on the solid-liquid interface in a dilute SCN-acetone alloy also at the limit of constitutional undercooling [29]. That elongated cells may appear even in concentrated alloys was shown by Jamgotchian et al. in Pb-30wt% Tl [30].

All observations of elongated cells reported in the literature [17-30] were made with bulk samples at the limit of constitutional undercooling. Thin cell experiments with transparent organic substances can not show that the morphological transition from planar solid-liquid interface into cellular patterns take place by forming elongated cells prior to cylindrical ones. The presented results reveal that this intermediate stage of cell formation is not restricted to the low velocity limit of stability but occurs also at the limit of absolute stability. Whether nodes are also present here, can not be decided from these experiments as they might be to small for the resolution of our equipment.

CONCLUSIONS

The main conclusions of this work are as follows:

- Reducing the solute content of a binary SCN - Ar alloy results in a morphological transition from deep cylindrical cells to a planar growth front. This transition developed in three different stages: (i) deep cells of circular cross section changed into a mixed pattern of elongated and cylindrical cells, (ii) which changed further into low amplitude cells and (iii) finally into the planar front.
- At low and at high solidification velocities, relatively large areas with irregular appearance were observed. These areas revealed a substructure indicating the appearance of shallow cells. In this stage, cylindrical, elongated and shallow cells can coexist.
- The appearance of elongated cells was also observed a the low velocity limit as well as at the high velocity limit of stability.
- For the alloy with $\Delta T_0 = 235$ mK, the shallow cells disappeared with *decreasing and increasing* growth velocity. Thus it is concluded that the experiments were performed near the limit point of the neutral stability curve.
- Within the uncertainty of the material properties and the thermal gradient, the appearance of a transition from shallow perturbations into planar front correlated well with linear stability theory. The size of the shallow perturbations is in reasonably good agreement with the critical wave length for the onset of instability.

Acknowledgement

The authors are glad to acknowledge the enlightening discussions with C. Caroli, S.H. Davis, G. Faivre, Ch.-A. Gandin, P. Metzener and M. Rappaz. They are grateful to J. Stramke for substantial and competent assistance in performing the experiments. This work has been supported by the Deutsche Forschungsgemeinschaft under Lu 495/1, for which the authors are grateful.

References

1) W.W. Mullins, R.F. Sekerka, J. Appl. Phys. 35, 444 (1964)
2) S.R. Coriell, R.F. Sekerka, J. Cryst. Growth 61, 499 (1983)
3) W.J. Boettinger, S.R. Coriell, R.F. Sekerka, Mater. Sci. Eng. 65, 27 (1984)
4) W.J. Boettinger, S.R. Coriell, in *Science and Technology of t he Undercooled Melt* , eds. P.R. Sahm, H. Jones, C.M. Adam, (Martinus Nijhoff, Dordrecht, 1986) p. 81
5) M.J. Aziz, J. Appl. Phys. 53 , 1158 (1982)
6) G.J. Merchant, S.H. Davis, Phys. Rev. B, 40, 11140 (1989)
7) R.J. Braun, S.H. Davis, J. Cryst. Growth 112, 670 (1991)
8) G.J. Merchant, R.J. Braun, K. Brattkus, S.H. Davis, SIAM J. Appl. Math. 52, 1279 (1992)
9) D.A. Huntley, S.H. Davis, Acta Met. Mat. 41, 2025 (1993)
10) R. Trivedi, K. Somboonsuk, Acta Met. 33, 1061 (1985)
11) H. Esaka, W. Kurz, J. Cryst. Growth 72, 578 (1985)
12) M.A. Eshelman, V. Seetharaman, R. Trivedi, Acta Met. 36, 1165 (1988)
13) R. Trivedi, J.A. Sekhar, V. Seetharaman, Met. Trans. A 20, 769 (1989)
14) M.A. Chopra, Ph. D. Thesis, Rensselaer Polytechnic Institute, Troy, New York (1983)
15) A. Ludwig, W. Kurz, submitted to Acta Met. Mat.
16) A. Ludwig, W. Kurz, to be publish
17) D. Walton, W.A. Tiller, J.W. Rutter, W.C. Winegard, Trans. Met. Soc. AIME 203, 1023 (1955)
18) W.A. Tiller, J.W. Rutter, Can. J. Phys. 34, 96 (1956)
19) H. Biloni, Can. J. Phys. 39, 1501 (1961)
20) H. Biloni, G.F. Bolling, Trans. Met. Soc. AIME 227, 1351 (1963)
21) H. Biloni, G.F. Bolling, G.S. Cole, Trans. Met. Soc. AIME 236, 930 (1966)
22) D.W. Jones, Trans. Met. Soc. AIME 236, 936 (1966)
23) G.S. Cole, W.C. Winegard, J. Inst. Met. 92, 322 (1964)
24) L.R. Morris, W.C. Winegard, J. Crystal Growth 5, 361 (1969)
25) T. Sato, G. Ohiro, Trans. JIM 12, 285 (1971)
26) T. Sato, G. Ohiro, J. Crystal Growth 40, 78 (1977)
27) K. Shibata, T. Sato, G. Ohira, J. Crystal Growth 44, 419 (1978)
28) T. Sato, K. Ito, G. Ohiro, Trans. JIM 21, 441 (1980)
29) S.N. Tewari, M.A. Chopra, J. Crystal Growth 118, 183 (1992)
30) H. Jamgotchian, B. Billia, L. Capella, J. Crystal Growth 64, 338 (1983)